Broadband Excess Noise Estimation via Sample Distribution Field Calibration

Sérgio M. Jesus, Cristiano Soares, Miriam Romagosa, Irma Cascão, Ricardo Duarte, Friedrich Zabel, and Mónica A. Silva

Contents

Introduction 2
Methods 4
Environmental Data 4
Ship Traffic 6
Acoustic Recordings 7
Ocean Sound Modeling 8
Sample Field Calibration 8
Broadband Excess Noise Level 9
Results and Discussion 10
The Acoustic Data Set 10
Experimental Data and Model Statistics 12
Field Calibration 14
ENL Estimation 16
Conclusions 17
References 19

Abstract

The Marine Strategy Framework Directive (MSFD) of the European Union currently requires meaningful noise level-based indicators to be obtained either through field data observations or computer modeling. Acoustic recordings in the 20–1000 Hz frequency band were performed 6 h a day during June 2018 in three

S. M. Jesus (✉) · R. Duarte
LARSys, Universidade do Algarve, Faro, Portugal
e-mail: sjesus@ualg.pt; rjduarte@ualg.pt

C. Soares · F. Zabel
Marsensing Lda., Campus de Gambelas, Faro, Portugal
e-mail: csoares@marsensing.com; fredz@marsensing.com

M. Romagosa · I. Cascão · M. A. Silva
IMAR-OKEANOS, University of the Azores, Horta, Portugal
e-mail: mirian.r.verges@uac.pt; irma.ma.cascao@uac.pt; monica.silva.imar@gmail.com

A. N. Popper et al. (eds.), *The Effects of Noise on Aquatic Life*,
https://doi.org/10.1007/978-3-031-10417-6_71-1

moorings to the southwest of the Islands of Faial and Pico (Azores). Anthropogenic noise was modeled due to ship traffic drawn from AIS data, and environmental sound was attributed to wind. Comparing field and model data at these three locations allowed to introduce a field calibration procedure based on the linear transformation of sample distribution probability density functions in the sound pressure-level domain. The broadband version of the excess noise level (ENL) appears as the sum of the 1/3-octave bands transformed power over the data recording frequency band. The results show that field-calibrated broadband ENL sound maps are in line with the main shipping routes, fishing activity, and leisure paths in the area revealing; however a significant noise spread due to sound propagation conditions to the east and the southwest of the Faial-Pico Islands. Field-calibrated broadband ENL may be seen as a reliable quantity for establishing continuous anthropogenic noise pollution MSFD indicators.

Keywords

Ocean soundscape · Shipping noise · Excess noise level · Field calibration

Introduction

Ocean noise level worldwide was found to be increasing at an estimated rate of 3 dB/decade between 1950 and 2010, in line with the increase in shipping and GDP growth (Frisk 2012). The full impact of this ocean noise increase is still unknown, but evidence is piling up toward a deterioration of the marine habitat, the disruption of the life cycle of a number of endangered species, and biodiversity loss (Hildebrand 2009; Hawkins and Popper 2014; Williams et al. 2015; Erbe et al. 2019; Duarte et al. 2021).

Until recently, the focus of ambient noise studies was on its spatial correlation, coherence, and directivity, with the scope of reduction or elimination. The rising concern of impacts of ocean noise on marine species shifted the focus of ambient noise studies to the ocean sound level, classically defined as the sound pressure level (SPL) mapped into geographical coordinates, time, and frequency – the so-called sound maps. In practice, sound maps are obtained through computer modeling, in order to cope with the required time-space resolution for a meaningful representation, impossible to obtain otherwise by direct observation. Sound maps are, therefore, a fundamental tool for marine policies development/enforcement, identifying areas impacted with high sound levels when compared to others relatively protected, and to follow sound stress dynamical changes along time. Ocean sound was recently declared as an essential ocean variable by the Global Ocean Observation System (GOOS). In the recently published United Nations World Ocean Assessment report, a new full chapter was dedicated to trends on anthropogenic noise inputs into the marine environment (Sirovic et al. 2021).

Conceptually, there are at least two approaches for estimating ocean noise: one is by summing all the individual anthropogenic source contributions in any given point in space, and the other is by measuring ocean sound and "subtracting" the natural

background sound level. As we will see, both approaches have their own difficulties, flaws, advantages, and drawbacks.

The Marine Strategy Framework Directive (MSFD) is the European Union's main policy for marine life protection and conservation, aiming at achieving the good environmental status and its monitoring, along with protection policies which require identifiable and meaningful indicators (European Commission 2010). Descriptor 11 of the MSFD defines two indicators: one for impulsive noise and another for continuous noise. Depending on the context, these two components are often difficult to separate, which is a requirement for building suitable MSFD indicators. A recent proposal defines the excess noise level (ENL) which is the anthropogenic noise in excess of the natural background ambient sound as a possible basis for continuous noise indicator (Farcas et al. 2020). The idea behind ENL is that of determining the anthropogenic noise on top of the natural ocean sound normally present in the ocean. This, of course, requires a measurement (or an estimate) of the reference or baseline sound level without noise contamination which, nowadays, is practically impossible. This is particularly difficult in north Atlantic, which is the basin size region with the most intense and constant ship traffic in the world (Sirovic et al. 2021).

It is commonly assumed that the two main contributions to ocean sound in the band 20–1000 Hz are shipping noise and the sound generated by wind on the ocean surface. Therefore, sound maps use computer models to generate realistic approximations of these two sound fields taking as input environmental information such as bathymetry, water column temperature and salinity profiles, bottom characterization and wind speed estimates, as well as ship traffic information drawn from the Automatic Identification System (AIS). Acoustic propagation models have been used for obtaining three-dimensional (actually better described as N $\times$ 2D) deterministic representations of the shipping noise field (Colin et al. 2015; Soares et al. 2015; Skarsoulis et al. 2016). This is a very computation-demanding task, in particular for large areas with intense traffic, so an alternative was devised to represent ship location through a statistical distribution and thus reduce the computational burden (Kinda et al. 2017).

Sound maps obtained through numerical modeling are error prone due to inherent parameter uncertainties, model mismatch, and environmental/AIS data dropouts. Any direct acoustic observation should be a valuable resource, first for sound map validation and then for an eventual model adjustment. The process of integrating model and field data for sound maps' correction is known as "field calibration." The most common approach for field calibration assumes that environmental data used in acoustic propagation models is erroneous or incomplete and its adjustment allows for matching data and model (Farcas et al. 2020). Another alternative is to consider that the mismatch comes from the source level assumed for the ships cruising in the area and its estimation from the data itself would allow for a better match, as proposed in a simulation exercise in Jesus et al. (2017). Recently, the third approach directly calibrates the statistical distributions of the modeled field as proposed in Jesus et al. (2022). The validation of the gain provided by each field calibration approach, and how this gain extends for time periods and locations where there are no ground truth observations is a challenging task.

The objectives of this study are as follows: one is to provide evidence for broadband ENL estimation methodology and explore the possibility of its usage to support building a continuous noise indicator, and the other to propose a sample field calibration method to integrate measurements and modeled data, for extending a localized observation into a wider area, where there were no observations.

This work is supported on acoustic recordings performed in the 20–1000 Hz frequency band, 6 h a day during June 2018 at three locations close to the Faial-Pico Islands, in the Azores archipelago, a well-known habitat for over 20 cetacean species (Silva et al. 2014). This data set was evaluated and found to be biased in some frequency bands, so its usage for model calibration is questionable and only made possible after filtering and conditioning. Ocean sound modeling was performed for ship traffic and surface wind action. The linear probability density functions' sample field calibration procedure presented in Jesus et al. (2022) was used and applied to this data set, extending the results with complimentary material in the following aspects: time and spatial evolution of water column; field calibration procedure is detailed; statistics for the worst-case recorder (MG) are shown; non-calibrated and calibrated model data detailed for all bands; and distribution means and variance before and after calibration.

Methods

Environmental Data

The Azores archipelago is formed by a total of nine islands in three groups: the western group of two islands, the eastern group of also two islands, and the central group composed of five islands, four of which are shown in Fig. 1 with the island of Graciosa to the north (not shown). The bathymetry data was obtained from the GEBCO (General Bathymetric Chart of the Oceans, www.gebco.net) database (Group, G.B.C 2020). The horizontal lines and the star symbol denote the locus for water column temperature and salinity information as shown in Fig. 2. The star

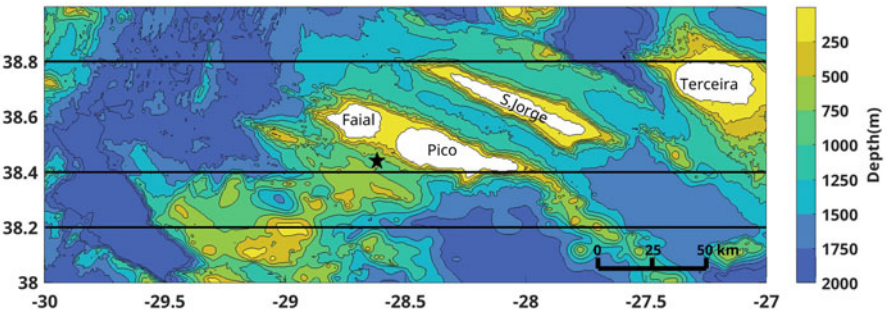

Fig. 1 Central group of islands of the Azores archipelago. The horizontal lines and black star indicate positions for extracting water column information as shown in Fig. 2 (Adapted from Jesus et al. 2022). Bathymetry data credits: GEBCO database (Group, G.B.C 2020)

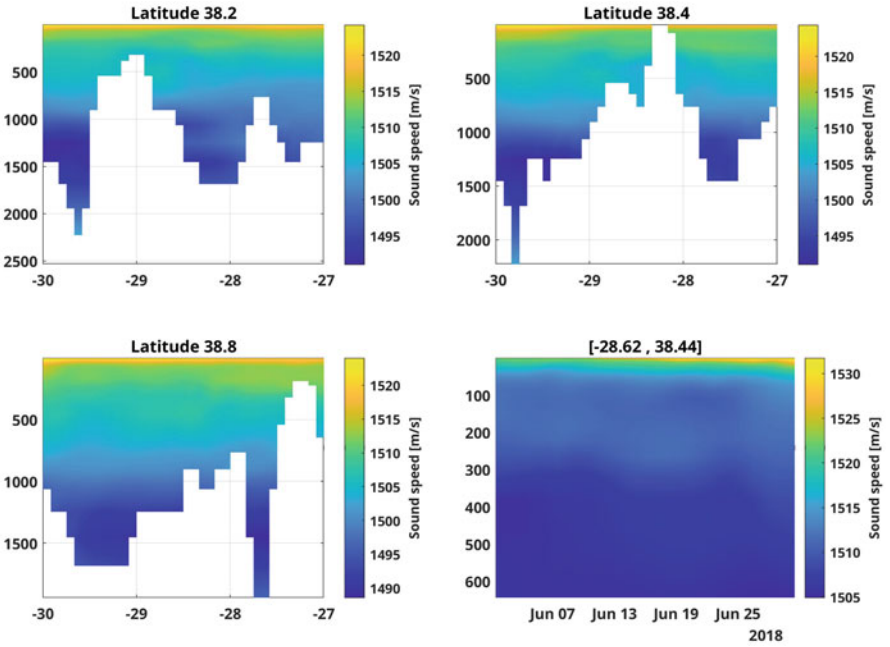

Fig. 2 Depth-longitude sound speed for latitudes of 38.2°, 38.4°, and 38.8° North calculated from temperature and salinity profiles, upper left, right, and bottom left plots, respectively, and sound speed time evolution through the month of June 2018 at location [−28.62 W – 38.44 N] (bottom right). (Source: CMEMS-Copernicus Marine Service)

symbol is in the vicinity of the acoustic recorders' location (see Fig. 5 for a close-up). The area under study is characterized by deep water with two main features: the shallow channel between Faial and Pico islands, with an average depth of approximately 80 m, and the shallow banks (<200 m depth) to the southwest of Faial Island, known as an important fishing area. Figure 2 shows computed sound speed using the temperature and salinity profiles extracted from the CMEMS (Copernicus Marine Environment Monitoring Service) (www.copernicus.eu) database, along constant latitude lines 38.2, 38.4, and 38.8, upper left, right, and bottom left plots, respectively, and for the sound speed evolution through time (bottom right plot) at the position indicated with the star symbol. Water column sound velocity variation with range is mild, as well as throughout the month of the study.

Figure 3 shows the wind speed over the month of June 2018 as predicted by the ECMWF (European Centre for Medium-Range Weather Forecasts, www.ecmwf.int) (Hersbach et al. 2018) for the mean (a) and the standard deviation (b). There is a significant deviation of more than 2 km/h from south to north of the considered area, while the standard deviation slightly decreases from west to east.

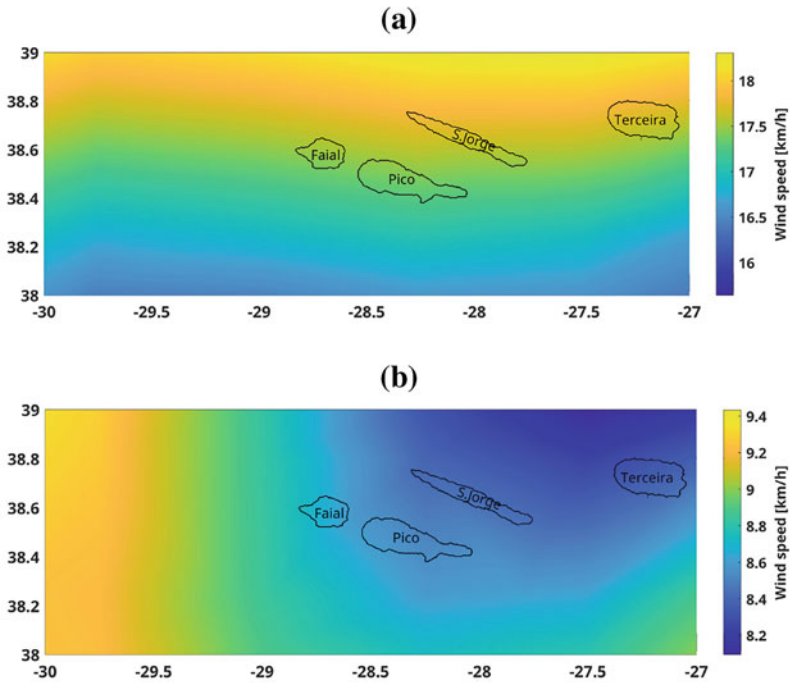

Fig. 3 Azores wind speed for June 2018: mean (**a**) and standard deviation (**b**) (Source: ECMFW (Hersbach et al. 2018). Plot (**a**) reprinted from (Jesus et al. 2022))

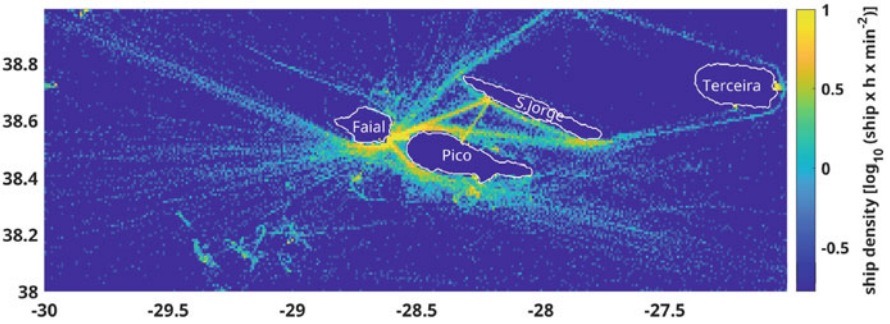

Fig. 4 Cumulative ship density for the month of June 2018 (Source: AISHub. Figure reprinted from Jesus et al. (2022))

Ship Traffic

Figure 4 shows the cumulative ship distribution as recorded on the community-shared platform AISHub (ship Automatic Identification System data exchange, www.aishub.net) for the study area during the whole month of June 2018. The

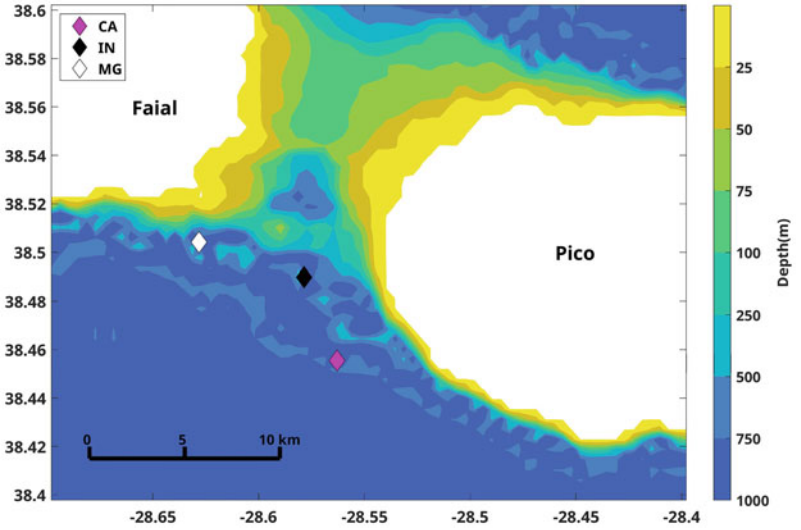

Fig. 5 Detailed bathymetry with recorders' location on the Pico side (CA), in the channel (IN), and on the Faial side (MG). Recorder's depths are 484 m for CA and 200 m for IN and MG

month of June was chosen since it approximately coincides with a period of high probability of the presence of cetaceans in the area. Data is shown as logarithm base 10 of ship density evaluated in ship x hour per square arc minute. That is, two ships for half an hour each on a square of approximately 1 nautical mile side will give rise to a ship density of 1 and will therefore appear as 0 in this figure.

Acoustic Recordings

Three ecological acoustic recorders (EARs) (Lammers et al. 2008) were positioned at the locations CA, IN, and MG shown in Fig. 5. The EARs are deep water-rated recorders for long-term deployment with a sensitivity between −193 and −194 dB re 1 V/μPa over the band 20–1000 Hz. During this experiment the data was sampled at 2000 Hz, with a 16-bit resolution and a 47.5 dB total chain gain. Antialiasing was achieved thanks to the usual low-pass filter to avoid out-of-band energy contamination. A high-pass filter was set at 20 Hz to attenuate static pressure low-frequency oscillations. SPL was estimated from 1 s duration Hann-windowed intervals with 50% overlap using the PAMGuide tool (Merchant et al. 2015) running under MATLAB® which is commonly used in the soundscape community. (See (Merchant et al. 2015) supplementary information with MATLAB® and R codes.) The three recorders at locations CA, IN, and MG were moored at depths of 484, 200, and 200 m, respectively. The received data was averaged in 10-min intervals and integrated over 1/3-octave (base 10) sub-bands in the 40–1000 Hz frequency band.

Ocean Sound Modeling

Ocean sound modeling was performed for the shipping noise and wind sound components in the frequency band 40–1000 Hz. Thus, model sound-level output L_m may be written as

$$L_m(t,f,\mathbf{r}) = 10 \ \log_{10}\left[\sum_{q=1}^{Q_t} 10^{\left[L_{Hq}\left(t,f,\mathbf{r};\mathbf{r}_q\right)+L_{Sq}(f)\right]/10} + 10^{L_w(t,f,\mathbf{r})/10}\right], \qquad (1)$$

where the first term represents the noise level due to a distribution of Q_t contributing ship sources of the individual level $L_{Sq}(f)$ (in dB) propagated from the qth source with a propagation loss $L_{Hq}(t, f, \mathbf{r}; \mathbf{r}_q)$ (also in dB) between source location $\mathbf{r}_q$ and receiver location $\mathbf{r}$ and L_w is the surface wind-generated sound level also in dB, all for time t, frequency f, and location $\mathbf{r}$ (latitude, longitude, and depth). Note that in this formulation L_{Hq} is taken as negative, since it represents the sound loss along the propagation path. Even acknowledging that the RANDI model is now widely used for source-level modeling (Breeding et al. 1996; MacGillivray and de Jong 2021) for a matter of simplification a lookup table-style source-level model for coefficient L_{Sq} was used, deduced from historical measurements according to ship type from (McKenna et al. 2012). A high number of contacts of sailing vessels was found in the AIS data, and the adopted procedure was that of assigning them to a source level of 1% of that of cargos ≈ 20 dB (see Soares et al. (2020) for details). Source depth for the various ship types was set according to Scrimger and Heitmeyer (1991). Transmission loss is estimated with the Kraken normal mode model (Porter 1991) using the environmental information described in section "Environmental Data." Due to the typical deep water propagation conditions of the area, bottom properties are expected to play a minor role. Therefore, a generic bottom composed of a 10-m-thick sediment layer over a semi-finite hard rock half space was used (see Soares et al. (2015) for detailed properties).

The wind sound model was deduced from the ECMWF database (Hersbach et al. 2018) using the data set shown in the previous section, and the method proposed by Kewley et al. (1990) assumes that the sound generated at the sea surface results from a two regime mechanism: below 8–10 km of wind speed at low sea state and one above that speed involving the formation of white caps. The laborious step of estimating the wind source level is described in detail in the companion paper (Jesus et al. 2022).

Sample Field Calibration

According to the sound model constraints and simplifications set above, the standard procedure for field calibration follows by estimating sound maps in 1/3-octave (base 10) frequency bands, represented by their center frequencies. At each center

frequency, the SPL time samples over the whole month are sorted into 1 dB bins to form histograms for both data observations and model predictions.

The sample field calibration procedure proposed in Jesus et al. (2022) is based on a linear variable transformation from the model to the data distribution, as described in more detail as follows. Let us assume that $p(L_m)$ and $p(L_d)$ are the model and the data distributions, with means and variances, respectively, given by $\left(\mu_m, \sigma_m^2\right)$ and $\left(\mu_d, \sigma_d^2\right)$. We seek to determine a model-calibrated distribution $p(L_{mc})$ drawn from the model samples, but with the same mean and variance than $p(L_d)$, by the linear scale transformation

$$L_{mc} = AL_m + B. \tag{2}$$

It can be easily found, from the identification between means and variances of $p(L_{mc})$ and $p(L_d)$, that $A^2 = \sigma_d^2/\sigma_m^2$ and that $B = \mu_d - A\mu_d$ which when inserted in (2) allow to determine the change scale of L_{mc} and therefore the calibrated distribution $p(L_{mc})$. Calibration coefficients will be determined for each 1/3-octave band, so that the full calibration map will be obtained through the coefficient set $\{A(f_k), B(f_k); k = 1, \ldots, K\}$, where K is the number of frequency bands. However, as we will see below, it is not sufficient to have the calibrated distributions, since in order to obtain a broadband estimate, the actual sample pressure power field needs to be summed across band. Replacing the levels in (2) by their respective pressure power definitions $L_* = 10\ \log_{10} P_*$ and solving for the calibrated power P_{mc} give

$$P_{mc} = P_m^A 10^{B/10}, \tag{3}$$

which allows to transform power samples according to the calibration mapping.

When the acquired data is hardware calibrated, validated, and free of interferences and self-noise, the proposed sample field calibration may be useful for correcting model systematic biases through the adjustment of the model data distribution mean and variance. This applies to the time intervals and recording locations where the data is gathered, which gives no guarantees for the validity of the correction coefficients for other areas or time frames. The domain of validity of the calibration set depends on a number of factors and, in particular, on the origin of the data-model mismatch.

Broadband Excess Noise Level

ENL is defined as the difference (in dB) between the measured and the baseline SPL for a given time, frequency, and space coordinates, expressed as

$$L_E(t,f,\mathbf{r}) = L_T(t,f,\mathbf{r}) - L_b(t,f,\mathbf{r}), \tag{4}$$

$$= 10 \ \log_{10} \frac{P_T(t,f,\mathbf{r})}{P_b(t,f,\mathbf{r})}, \tag{5}$$

where in (4), L_E is the ENL, L_T is the total sound level, and L_b is the baseline ocean sound level without anthropogenic pressures. Relation (5) is readily obtained by replacing sound levels L_T and L_b by its respective pressure power counterparts P_T and P_b, using $L_* = 10 \ \log_{10} P_*$. The total sound level L_T is drawn either directly from observation or as the modeled sound level L_m given in (1). The baseline (or background) ocean sound level is normally obtained from the modeled wind sound level L_w (or the P_w pressure power). Thus, replacing $P_T = P_S + P_w$, where P_S is the shipping term power, and $P_b = P_w$ in (5) allows to rewrite ENL as

$$L_E(t,f,\mathbf{r}) = 10 \ \log_{10} \left[1 + \frac{P_s(t,f,\mathbf{r})}{P_w(t,f,\mathbf{r})}\right]. \tag{6}$$

Under these assumptions, the instantaneous ENL given by (6) will be always ≥ 0, as expected, and takes into account noise and baseline estimates modeled at a given time and location. Alternatively, the baseline level could be defined as a mean over time, in which case $P_w(t,f,\mathbf{r})$ in (6) would be replaced by the mean $\overline{P}_w(f,\mathbf{r})$. Even in that case L_E remains always ≥ 0.

The expression above denotes ENL for a single frequency or for a narrow 1/3-octave band around a center frequency f_k. Extending this to the broadband case implies power summing (and not power averaging as was proposed in Farcas et al. (2020)) over the required bands so, in that case, the definition for broadband ENL would be given by Jesus et al. (2022)

$$L_E(t,\mathbf{r}) = 10 \ \log_{10} \left[\frac{\sum_{k=1}^{K} P_T(t,f_k,\mathbf{r})}{\sum_{k=1}^{K} P_b(t,f_k,\mathbf{r})}\right], \tag{7}$$

where K was already defined as the number of frequencies or bands. This definition allows to take into account a ratio of energies which are the preferred quantities for determining indicators of harm to marine life.

Results and Discussion

The Acoustic Data Set

Figure 6 shows the spectral probability densities for the received data at the three locations CA, IN, and MG in plots (a) to (c), respectively. Each vertical line is a normalized sample count color-coded image of a data histogram in 1 dB slots, for 1 Hz bin. Each frequency bin is obtained as the sample power spectrum (without averaging) of 1 s duration intervals with 50% overlap throughout the whole month. With this setting, clear colors denote most probable levels and dark colors the least

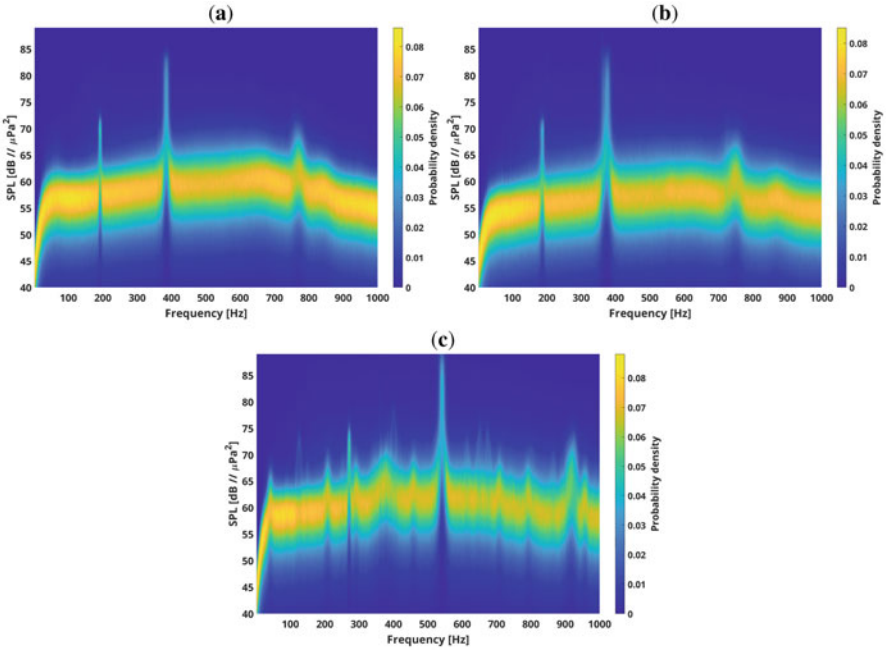

Fig. 6 Spectral power distribution with 1 s, 50% overlap time slots between 14:00 and 20:00 UTC in June 2018 for recorders at sites CA (**a**), IN (**b**), and MG (**c**) (Figure reprinted from Jesus et al. 2022)

Table 1 Recorder's self-noise filtered bands

Recorder sites	Bands [Hz]
CA	[188–197], [374–393]
IN	[184–192], [357–387]
MG	[267–274], [528–553]

probable, across the frequency band. This figure shows a clear cut-off frequency at 20 Hz for the three recorders, followed by a slight and progressive SPL increase with frequency until approximately 300 Hz. This is the most relevant frequency band for shipping noise. The few spurious high-level peaks present in recorders CA (a) and IN (b) and in large number in recorder MG (c) are believed to be associated to recorders' self-noise. The origin of these peaks is actually unknown but believed to be related to some defecting amplifier or other components in the signal chain. This is clearly an issue on the quality of this particular data set and suggests precautions before its usage for field calibration. Therefore, the focus of this paper is not so much on the final calibrated field result but on showing and detailing the methodology employed for obtaining the result. Nevertheless, the impact of these peaks may be mitigated by filtering the frequency bands clearly off the mean level. The following procedures were adopted: (1) first detect the two highest peaks and (2) filter out the bins of the surrounding frequency band for each recorder of Fig. 6, leading to the

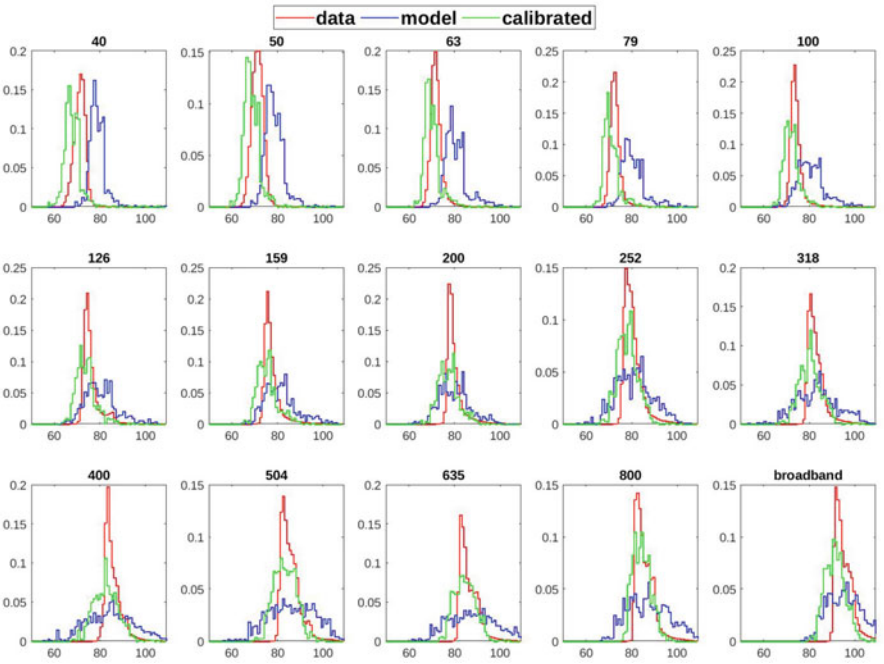

Fig. 7 SPL histograms for 1/3-octave bands (base 10) and broadband (bottom right), using 1 s time slots with 50% overlap, between 14:00 and 20:00 UTC in June 2018 for recorder location MG positioned at 200 m depth: recorded data (red), shipping and wind model-generated data (blue), and field-calibrated model (green) [axes: probability density (y) in 1 dB re 1 μPa, SPL bins (x)]

result in Table 1. The proposed filtering is not a definitive response to the self-noise impairments found in the data and just attempts to mitigate its effects without compromising the field calibration broadband ENL estimation technique.

Experimental Data and Model Statistics

Figure 7 shows histograms of the observed data (red), shipping and surface wind sound-modeled data (blue), and field-calibrated data (green) for the MG recording location at the 1/3-octave (base 10) frequency bands between 40 and 1000 Hz. The corresponding broadband field histograms (bottom right plot) are also shown. The MG recorder corresponds to the worst-case self-noise according to the spectral power distributions of Fig. 6. Similar results were obtained for locations CA and IN (not shown). The field-calibrated distributions (in green) were obtained with the proposed method (see section "Sample Field Calibration") with a modification explained as follows. For this case, the data adjustment coefficients $\{A, B\}$ were calculated not independently for the data sets gathered at each location but, instead, from the data samples merged from all three data sets at locations CA, IN, and MG

pulled together. This allows for the inclusion of all the observed data in the calibration method, thus providing a higher spatial and temporal robustness than by using sensors individually. This procedure also solves the problem of deciding which area or time interval to calibrate with each sensor. The data merging is also justified by the fact that the three sensor's location may be seen as a single point in the full study area (Fig. 1). The direct result of this merging is that the calibrated distributions are not exactly matched (mean and variance) to any of the data sets. This is illustrated in Fig. 7, for the case of MG, as a slight mismatch between green and red curves. That mismatch is also clear in the broadband case (bottom right plot). Note that in that case, the calibrated broadband distribution is obtained as the sample's sum over frequency and not from a direct calibration between the (broadband) model and data histograms.

The observed data statistical SPL distributions for the 1/3-octave (base 10) bands (Fig. 7 red curves) show a relatively narrow probability density function with a variable mean in frequency and self-noise limited low levels, either due to insufficient gain or poor resolution. As mentioned above, these histograms were obtained after filtering the frequency bands of the two main peaks of the spectral probability densities for each recorder of Fig. 6. Empirical probability density functions for the modeled ocean sound field were obtained for the same setup parameters as the data, i.e., for the recorder coordinates (latitude, longitude, and depth) and for the same time frames (Fig. 7 blue curves). In general, the model SPL distributions tend to overestimate the data in the low-frequency band until roughly 150 Hz, while a better model data fit is obtained above that frequency. In some cases, the model data distribution is bimodal or multimodal, which is also found in the observed data, but with a much larger variance in the model than in the data. Whether that multimodality comes from ship traffic at different times, distances, or ship types is unclear. No apparent low-level threshold is found in the modeled data. The high probability peaks larger in the data than in the model are simply due to probability density surface normalization. The differences between data and model were used as the basis for the proposed field calibration method for the wider area even if the real data recording conditions were not ideal.

The next step is to enlarge the modeling area to the four Islands shown in Fig. 1. A sampling interval of 10 min and a spatial grid of square size of 500 m were chosen for computing the wide area sound map. There is no consensus regarding receiver depth for sound models, so 10 m was chosen to represent a depth near the surface at which large whales spend a significant amount of time, and it was also noticed that, for this data set, this depth generally corresponded to the worst-case depth (highest level in general) among the various tests performed. Figure 8 shows the model's estimated mean SPL field for each 1/3-octave band (base 10) in 40–1000 Hz and the broadband case (bottom right plot) for the whole area. The same color scale is used for all frequency bands, including the broadband plot (bottom right). As expected, levels are lower for the lower bands and tend to increase with frequency. Noise peaks up to over 120 dB can be noticed in the channel between Faial and Pico and out of the port of Terceira. Shipping routes are apparent between Faial or Pico to S. Jorge and Terceira Islands, as well as other paths to other islands (out of the area). High

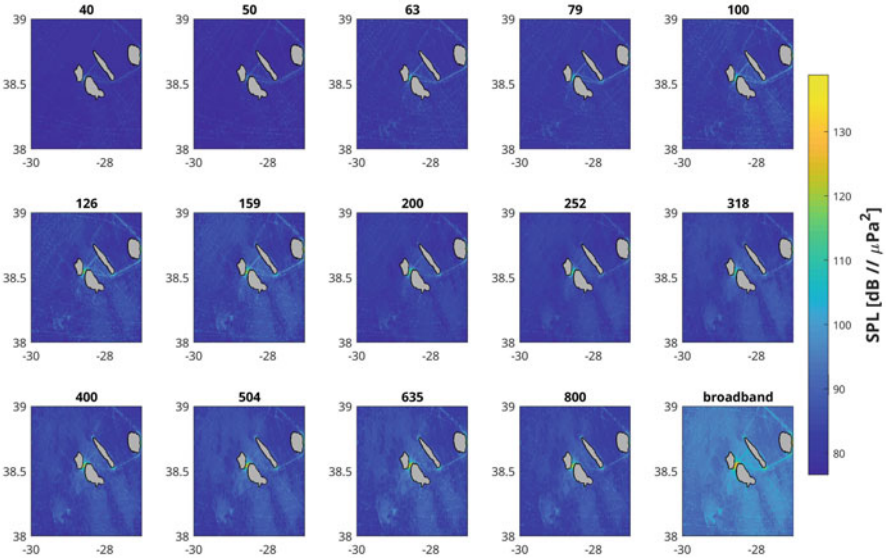

Fig. 8 Mean SPL for the 1/3-octave band's (base 10) center frequencies in 40–1000 Hz and broadband field (bottom right plot), at 10 m depth for June 2018 [axes: latitude (y), longitude (x) both in decimal arc degrees] (Figure reprinted from Jesus et al. 2022)

SPL areas spreading out from these routes can be seen to the southeast of Faial-Pico-S. Jorge and in the shallow banks to the southwest, which is possibly due to the already mentioned fishing activity in the area.

Field Calibration

The sample calibration method outlined in section "Sample Field Calibration" with the data-dependent modifications set forth in the previous section, illustrated for the MG location in the distributions of Fig. 7, was applied to the modeled data at the recorder locations for verification and then extended to the wide area and for the complete month. Figure 9 shows the frequency evolution of the mean (a) and standard deviation (b) of the sample distributions averaged over the three recorders for data (continuous blue), model prediction (continuous brown), and calibrated separately for CA, IN, and MG (dashed). As expected, there is a clear adjustment in mean and standard deviation from model to data procured by the calibration method. This adjustment is slightly better for IN than for MG and CA recorders. Model predictions overestimate the data over the whole band but more at low frequency (below 200 Hz). The mean absolute error between model and data is in the order of 6.8 dB for the whole data reduced, after calibration, to 3.9 dB.

Applying the calibration to the wider area allows to obtain the mean SPL results shown in Fig. 10 for the 1/3-octave band center frequencies and the whole month of

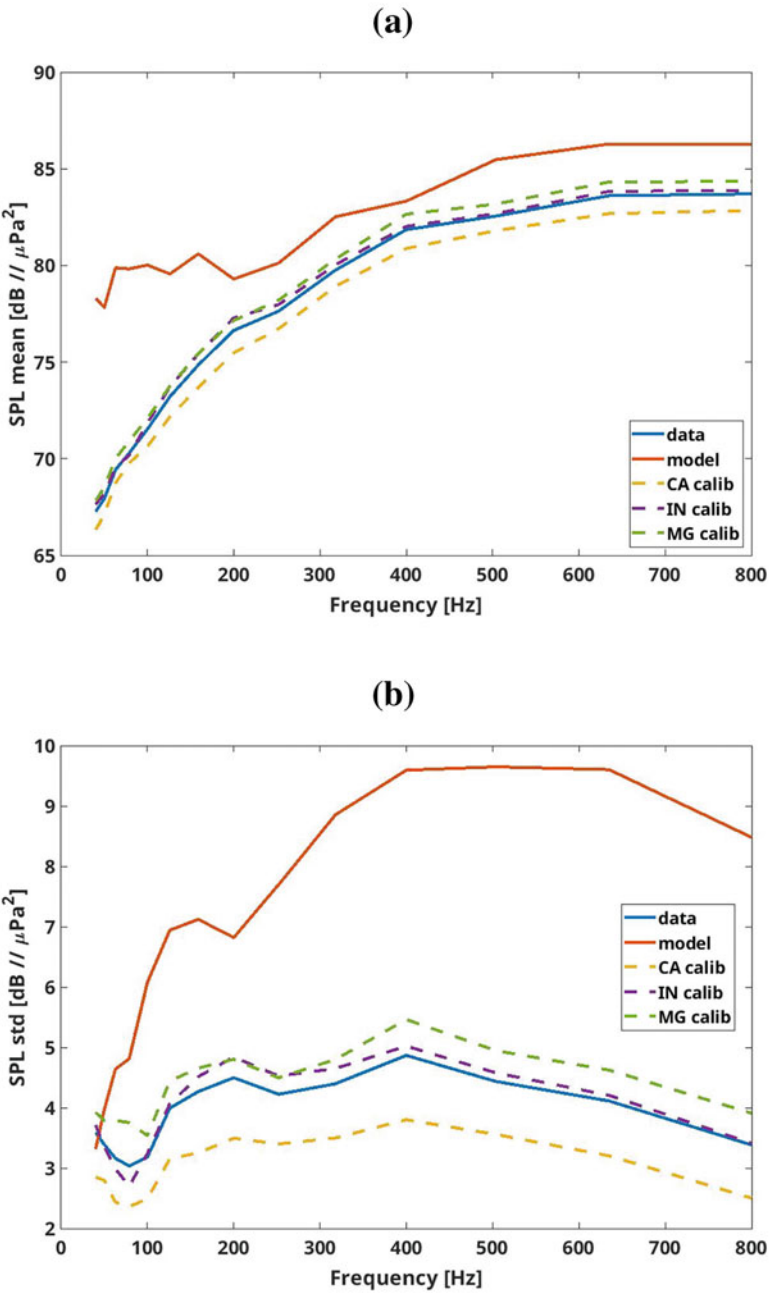

Fig. 9 Sample distribution's SPL mean (**a**) and standard deviation (**b**) averaged over the three recorders for data (continuous blue), model prediction (continuous brown), and calibration separately shown for CA, IN, and MG (dashed) versus 1/3-octave band (base 10) center frequencies

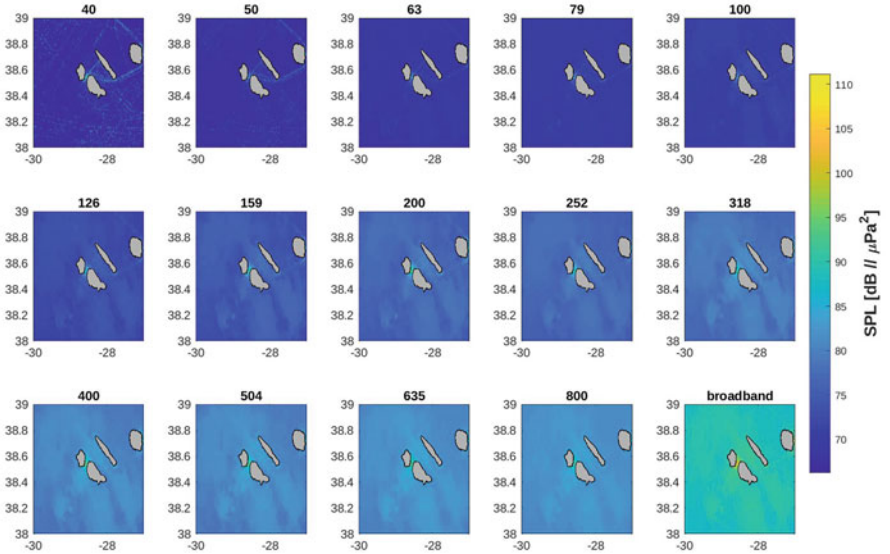

Fig. 10 Field-calibrated mean SPL for the 1/3-octave band (base 10) center frequencies in 40–1000 Hz using (6) and broadband using (7) (bottom right plot), at 10 m depth for June 2018 [axes: latitude (y), longitude (x) both in decimal arc degrees]

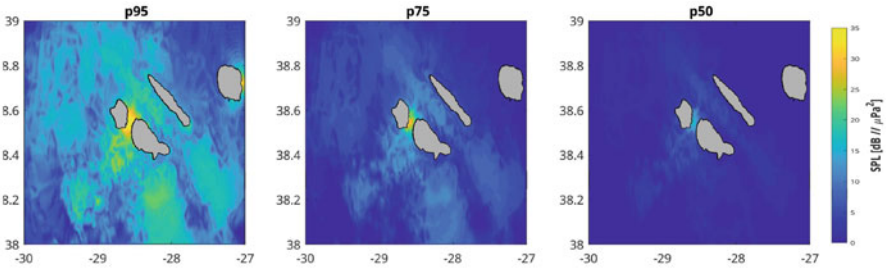

Fig. 11 Model predicted instantaneous broadband excess noise level (ENL) 95, 75, and 50 percentiles in the 40–1000 Hz band at 10 m depth for the whole area, in June 2018 with a spatial and time resolution of 500 m and 10 min, respectively [axes: latitude (y), longitude (x) both in decimal arc degrees] (Figure partially reprinted from Jesus et al. 2022)

June 2018. As expected, levels are overall lower than before calibration, and surfaces are flatter, because variance has, in general, been reduced.

ENL Estimation

The wind model is used as baseline for estimating the instantaneous ENL using definition (6) and in its broadband form using (7). Figure 11 shows the 95, 75, and 50 percentiles of the broadband instantaneous ENL field at 10 m depth before

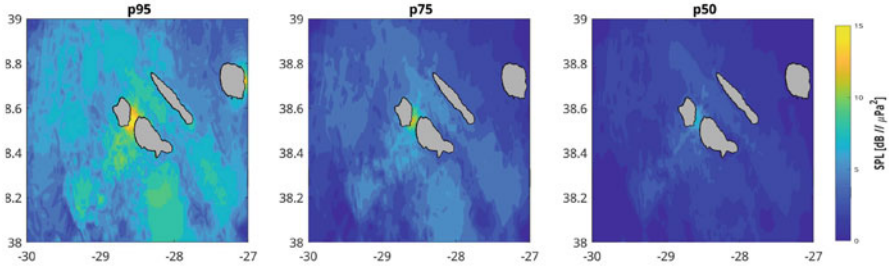

Fig. 12 Field-calibrated predicted instantaneous broadband excess noise level (ENL) 95, 75, and 50 percentiles in the 40–1000 Hz band at 10 m depth for the whole area, in June 2018 with a spatial and time resolution of 500 m and 10 min, respectively [axes: latitude (y), longitude (x) both in decimal arc degrees] (Figure partially reprinted from Jesus et al. 2022)

calibration. ENL values up to 35 dB re 1 μPa^2 were estimated in the channel between Faial and Pico Islands and from 15 to 25 dB in extensive regions away from the islands but only for 5% of the time.

Figure 12 shows the predicted ENL statistics for the same parameters as in Fig. 11 but using the $\{A, B\}$ field calibration coefficients deduced from the observed data merged for the three recorders, as explained above. The calibration process tends to approach the model to the data, imposing lower mean levels in the lower-frequency bands and narrower distributions (smaller variances), which is consistent with the differences between Figs. 11 and 12. There are a few ENL high peaks reaching over 15 dB at the usual locations (channel between Faial and Pico) and only for small time periods (5% and 25% of the month). Comparison of figures before and after calibration shows an ENL mean decrease of approximately 8 dB re 1 μPa. The validation of the calibration process is not an easy task due to the lack of observations both in time and space. For example, the area that extends from the channel between Pico and S. Jorge to the south and northeast shows prevailing noise levels that are difficult to objectively validate. We may speculate that these levels, which occur in a small portion of the time, might be associated with the shipping lane to Terceira that encounters favorable propagation. Thus, it can be put forward that the proposed calibration methodology provides a balanced adjustment for systematic modeling errors coherent with patterns of the study area. One of the features of the proposed calibration method is that it is based on a statistical behavior of the data in user-defined time lapses of the available data sets and thus perfectly adaptable to other areas and periods of the year.

Conclusions

The Azores is an important habitat for cetaceans, but it is also a crossroad of several long-haul shipping routes, and a significant part of its economy is based on marine traffic around and between islands (ferries, leisure boats, small cargo and fishing).

The ship traffic density around the islands shows some long well-identified routes between islands and from the islands to other destinations outside of the study area. There is also some traffic scattered well away of the islands, probably due to intercontinental traffic. Local ships connect close by ports for small leisure trips, ferries, or fishing. Noise propagates away from intense shipping lanes if and when acoustic propagation conditions are favorable. Marine traffic produces ocean noise that impacts on marine species. The Azores is also challenging for acoustic monitoring because it is a vast deep ocean area with a few islands for supporting permanent monitoring buoys or platforms.

Acoustic data recordings at the three locations to the southwest of the islands of Faial and Pico are in general coherent with AIS ship traffic density in the area. Assuming that model data may be systematically biased, field calibration is extended to a larger area covering four islands of the Azores archipelago for the full month of June 2018. The results show that field-calibrated broadband ENL sound maps are coherent with the ship traffic in the study area, revealing a number of potentially threatening hotspots due to sound propagation conditions off shipping routes and vessel traffic patterns between islands.

The validation of the results is an impossible task without the help of additional direct observations in space and time. However, the proposed broadband ENL formulation seems to give a good superposition with the estimated marine traffic activity in and around the central Islands of the Azores archipelago. More surprising were the vast areas of high ENL to the southeast of the central islands that can be asserted to sound spreading from the shipping routes from these islands to/from Terceira. However, intense spreading in this area only occurs for a small portion of the time, at least during the considered month. The attempt for using localized data for calibrating model predictions in the wide area produced two effects: one was the overall ENL reduction and the other a decrease in the dispersion for most of the time. However, the areas with higher ENL are consistent with direct observation of shipping. Although there is no other comparable study for this area, excess levels seem to be relatively low ($<$10 dB, 50% of the time) during the study period. It is possible that the wide area might be too large for an effective calibration with only three recorders relatively close to each other.

Acknowledgments The work reported in this manuscript was funded under project JONAS (grant EAPA 52-2018, INTERREG Atlantic program of the European Union). Collection of acoustic data was funded by the Portuguese Science & Technology Foundation (FCT) through research project AWARENESS-PTDC/BIA-BMA/30514/2017 (FEDER, COMPETE, QREN, POPH, ESF, PORLisboa, Portuguese Ministry for Science and Education). MR was funded by DRCT (grant M3.1.a/F/028/2015), IC by FCT-IP Project (grant UIDP/05634/2020), and MAS by AZORES 2020, through the EU Fund 01-0145-FEDER-000140 "MarAZ Researchers: Consolidate a body of researchers in Marine Sciences in the Azores", and Okeanos by FCT (grant UIDB/05634/2020). We thank Marc Lammers and Sérgio Gomes for their technical support with the EARs.

References

Breeding JE, Pflug LA, Bradley M, Walrod MH, McBride W (1996) Research Ambient Noise DIrectionality (RANDI) 3.1 physics description. Technical report NRL/FR/7176-95-9628. Naval Research Laboratory, Stennis Space Center, Hancock

Colin M, Ainslie M, Binnerts B, de Jong C, Karasalo I, Ostberg M, Sertlek HO, Folegot T, Clorennec D (2015) Definition and results of test cases for shipping sound maps. In: Proceedings of the IEEE/MTS Oceans'15, Genova, June 2015

Duarte CM, Chapuis L, Collin SP, Costa DP, Devassy RP, Eguiluz VM, Erbe C, Gordon TAC, Halpern BS, Harding HR et al (2021) The soundscape of the Anthropocene ocean. Science 371: eaba4658. https://doi.org/10.1126/science.aba4658

Erbe C, Marley SA, Schoeman RP, Smith JN, Trigg LE, Embling CB (2019) The effects of ship noise on marine mammals – a review. Front Mar Sci 6:606. https://doi.org/10.3389/fmars.2019.00606

European Commission (2010) On criteria and methodological standards on good environmental status of marine waters. Off J Eur Union, tex.number: 2010/477/EU, Brussels

Farcas A, Powell CF, Brookes KL, Merchant ND (2020) Validated shipping noise maps of the Northeast Atlantic. Sci Total Environ 735:139509. https://doi.org/10.1016/j.scitotenv.2020.139509

Frisk GV (2012) Noiseonomics: the relationship between ambient noise levels in the sea and global economic trends. Sci Rep 2:437. https://doi.org/10.1038/srep00437

Group, G.B.C (2020) The GEBCO_2020 Grid – a continuous terrain model of the global oceans and land. Medium: network common data form version number: 1 type: dataset. https://doi.org/10.5285/A29C5465-B138-234D-E053-6C86ABC040B9. Accessed Nov 2021

Hawkins A, Popper A (2014) Assessing the impact of underwater sounds on fishes and other forms of marine life. Acoust Today 10:30–41

Hersbach H, Bell B, Berrisford P, Biavati G, Horányi A, Muñoz Sabater J, Nicolas J, Peubey C, Radu R, Rozum I et al (2018) *ERA5* hourly data on single levels from 1979 to present. Technical Report Copernicus Climate, Change Service (C3S) Climate Data Store (CDS); C3S (EU). https://doi.org/10.24381/cds.adbb2d47

Hildebrand J (2009) Anthropogenic and natural sources of ambient noise in the ocean. Mar Ecol Prog Ser 395:5–20. https://doi.org/10.3354/meps08353

Jesus S, Soares C, Zabel F (2017) Shipping noise field calibration via source inversion. In: Proceedings of the IEEE MTS/OES Oceans 2017, Aberdeen, June 2017

Jesus SM, Soares C, Romagosa M, Cascão I, Duarte R, Zabel F, Silva MA (2022) A methodology for shipping noise field calibration and excess noise estimation: the Azores case study. J Mar Sci Eng 10(11):1763. https://doi.org/10.3390/jmse10111763

Kewley DJ, Browning DG, Carey WM (1990) Low-frequency wind-generated ambient noise source levels. J Acoust Soc Am 88:1894–1902. https://doi.org/10.1121/1.400212

Kinda GB, Le Courtois F, Stéphan Y (2017) Ambient noise dynamics in a heavy shipping area. Mar Pollut Bull 124:535–546. https://doi.org/10.1016/j.marpolbul.2017.07.031

Lammers MO, Brainard RE, Au WWL, Mooney TA, Wong KB (2008) An ecological acoustic recorder (EAR) for long-term monitoring of biological and anthropogenic sounds on coral reefs and other marine habitats. J Acoust Soc Am 123:1720–1728. https://doi.org/10.1121/1.2836780

MacGillivray A, de Jong C (2021) A reference spectrum model for estimating source levels of marine shipping based on automated identification system data. J Mar Sci Eng 9:369. https://doi.org/10.3390/jmse9040369

McKenna M, Ross D, Wiggins S, Hildebrand J (2012) Underwater radiated noise from modern merchant ships. J Acoust Soc Am 131:92–103

Merchant N, Fristrup K, Johnson M, Tyack P, Witt M, Blondel P, Parks S (2015) Measuring acoustic habitats. Methods Ecol Evol 6:257–265. https://doi.org/10.1111/2041-210X.12330

Porter M (1991) The KRAKEN normal mode program, Number SM-245; Tex.Organization, Saclant Undersea Research Centre, La Spezia

Scrimger P, Heitmeyer RM (1991) Acoustic source-level measurements for a variety of merchant ships. J Acoust Soc Am 89:691–699. https://doi.org/10.1121/1.1894628

Silva MA, Prieto R, Cascão I, Seabra MI, Machete M, Baumgartner MF, Santos RS (2014) Spatial and temporal distribution of cetaceans in the mid-Atlantic waters around the Azores. Mar Biol Res 10:123–137. https://doi.org/10.1080/17451000.2013.793814

Sirovic A, Evans K, Garcia-Soto C, Hildebrand J, Jesus S, Miller J (2021) Trends in inputs of anthropogenic noise into the marine environment. In: World Ocean Assessment II, vol 2. United Nations, New York, pp 297–320

Skarsoulis E, Piperakis G, Orfanakis E, Papadakis P (2016) Prediction of shipping noise in the Eastern Mediterranean Sea. In: Proceedings of the INTER-NOISE'2016, Hamburg, Sept 2016, pp 329–336

Soares C, Zabel F, Jesus S (2015) A shipping noise prediction tool. In: Proceedings of the MTS/IEEE Oceans'15, Genova, June 2015

Soares C, Duarte RJ, Silva MA, Romagosa M, Jesus SM (2020) Shipping noise in the Azores: a threat to the Faial-Pico cetacean community? Proc Meet Acoust 40:070012. https://doi.org/10.1121/2.0001313

Williams R, Wright A, Ashe E, Blight L, Bruintjes R, Canessa R, Clark C, Cullis-Suzuki S, Dakin D, Erbe C et al (2015) Impacts of anthropogenic noise on marine life: publication patterns, new discoveries, and future directions in research and management. Ocean Coast Manag 115:17–24. https://doi.org/10.1016/j.ocecoaman.2015.05.021